

Helical Network Model for Twisted Bilayer Graphene

Dmitry K. Efimkin¹ and Allan H. MacDonald¹

¹The Center for Complex Quantum Systems, The University of Texas at Austin, Austin, Texas 78712-1192, USA

In the presence of a finite interlayer displacement field bilayer graphene has an energy gap that is dependent on stacking and largest for the stable AB and BA stacking arrangements. When the relative orientations between layers are twisted through a small angle to form a moiré pattern, the local stacking arrangement changes slowly. We show that for non-zero displacement fields the low-energy physics of twisted bilayers is captured by a phenomenological helical network model that describes electrons localized on domain walls separating regions with approximate AB and BA stacking. The network band structure is gapless and has a series of two-dimensional bands with Dirac band-touching points and a density-of-states that is periodic in energy with one zero and one divergence per period.

Introduction— The electronic structure of bilayer graphene is sensitive to strain, interlayer potential differences, and the stacking arrangement between layers [1, 2]. For the energetically favored Bernal stacking configurations, either AB or BA, Bloch states have 2π Berry phases, quadratic band-touching, and a gap that opens when a displacement field is applied by external gates. The gapped state is characterized by nontrivial valley-dependent Chern numbers and supports topological confinement of electrons on domain walls that separate regions with opposite signs of displacement field [3–6] or different stacking arrangements [7–9]. The presence of confined electronic states, which occur in helical pairs with opposite propagation directions in opposite valleys, has [10–12] been confirmed experimentally. Control of these domain walls and of their intersections has attracted attention recently [13–18] because of its potential relevance for valleytronics [19].

Whereas an engineering of a network of helical states with tunable geometry is a challenging problem, the triangular one has been recently observed [20] with help of scanning tunneling spectroscopy (STM) in misoriented graphene bilayers [21–40]. In the presence of a twist local stacking arrangement changes slowly in space in a periodic moiré pattern in which regions with approximate AB and BA stacking are separated by domain walls with helical states. The measured local density of states at a domain wall is strongly energy dependent with a single peak within the gap, that demonstrates the importance of an interference between helical states propagating along network. Because the moiré pattern is well developed only when its period greatly exceeds graphene’s lattice constant, theories of its electronic structure [41, 42] often employ complicated multi-scale approaches to advantage.

In this Letter, we derive a phenomenological helical network model for the electronic structure of gated bilayer graphene moirés valid in the energy range below the AB and BA gaps where only topologically confined domain wall states are present. The model is related to Chalker-Coddington type models [43–45] introduced in theories of the quantum Hall effect. The spectrum of the network model consists of a set of minibands con-

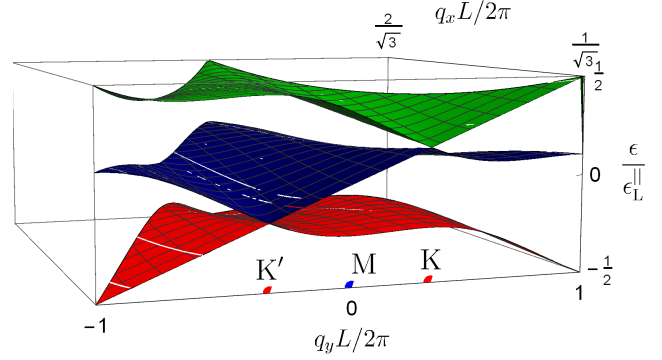


FIG. 1. Helical model band structure over half of the rhombic Brillouin zone (BZ) defined in Fig. 3-(c). The bands in the other half of the BZ can be obtained by the reflection. The model’s band energies $\epsilon_{\mathbf{q}}^{n0}$ are given by Eq. (10) and depend on a single controlling parameter α which was set to $\alpha = 1.1$ in this illustration. The bands touch at Dirac points located at high symmetry K, K’ and Γ points.

nected by Dirac band touching points, which repeats and is gapless. A single period of the model’s band structure is illustrated in Fig. 1.

Moiré pattern and helical states— To describe the electronic structure of gated bilayer graphene with a small twist angle $\theta \lesssim 1^\circ$ [46] between layers, we start from the continuum model Hamiltonian derived in Ref. [21], which is valid independent of atomic scale commensurability

$$H_0 = \begin{pmatrix} v\sigma_t \mathbf{p} - u & T(\mathbf{r}) \\ T^+(\mathbf{r}) & v\sigma_b \mathbf{p} + u \end{pmatrix}. \quad (1)$$

The Hamiltonian for a valley K acts in the sublattice space $\psi = \{\psi_A^t, \psi_B^t, \psi_A^b, \psi_B^b\}$, where t and b refer to the top and bottom layer, v is the single-layer Dirac velocity; $\sigma_{t(b)}$ is the vector of Pauli matrices rotated by the angle $\pm\theta/2$ in top and bottom layers, and $2u$ is the potential difference between layers produced by the gates. The spectrum is valley and spin independent, while electronic states in two valleys K and K' transform to each other by the time-reversal transformation. The inter-layer hop-

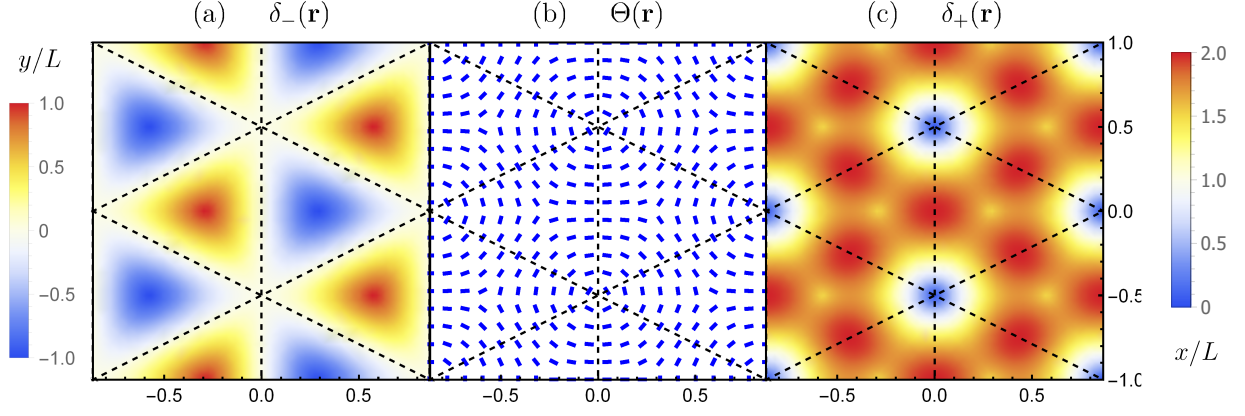


FIG. 2. Spatial distribution of the the gap parameters in Eq.(4): (a) the gap minimum δ_- ; (b) the angle $\theta(\mathbf{r})$ which specifies the direction in momentum space at which minima are achieved; (c) the gap maximum δ_+ . The dashed lines highlight the network of domain walls that separate regions in which the hybridization is dominated by T_{AB} from regions in which it is dominated by T_{BA} .

ping operator is given by

$$T(\mathbf{r}) = \frac{w}{3} \sum_{i=1}^3 e^{-i\mathbf{k}_i \cdot \mathbf{r}} T_i, \quad (2)$$

where w is a hybridization energy scale. The vectors $\mathbf{k}_1 = -k_\theta \mathbf{e}_y$, $\mathbf{k}_{2,3} = k_\theta(\pm\sqrt{3}\mathbf{e}_x + \mathbf{e}_y)/2$ all have magnitude equal to the twist-induced separation between the Dirac points of the two-layers, $k_\theta = 2k_D \sin(\theta/2)$ where $k_D = 4\pi/3a_0$ is the magnitude of the Brillouin-zone corner vector of a single layer and a_0 is the corresponding Bravais period. The matrices T_i are given by

$$T_1 = \begin{pmatrix} 1 & 1 \\ 1 & 1 \end{pmatrix}, \quad T_2 = \begin{pmatrix} e^{-i\zeta} & 1 \\ e^{i\zeta} & e^{-i\zeta} \end{pmatrix}, \quad T_3 = \begin{pmatrix} e^{i\zeta} & 1 \\ e^{-i\zeta} & e^{i\zeta} \end{pmatrix},$$

with $\zeta = 2\pi/3$. The inter-layer hopping operator in Eq.(2) is spatially periodic with the period of the moiré pattern $L = a_0/(2\sin(\theta/2))$.

The network model we derive has its widest range of applicability in the large gate voltage regime $\epsilon_L \ll u \sim w$ where $\epsilon_L = 2\pi\hbar v/L$ is the energy scale of the network mini-bands, as we explain below. In this limit an energy gap $\sim w$ develops around the momentum space ring of radius $p_u = u/v$ where the conduction band of the low potential top layer overlaps with the valence band of the high potential bottom layer. At energies $\epsilon \ll w$ the bilayer spectrum can be described by the projected two-band Hamiltonian

$$H = \begin{pmatrix} v(p - p_u) & t_P + t_S \\ t_P^* + t_S^* & -v(p - p_u) \end{pmatrix}. \quad (3)$$

In Eq. 3 we have separated the tunneling matrix element into two parts, an anisotropic part with p-wave symmetry $t_P(\phi_{\mathbf{p}}, \mathbf{r}) = [T_{BA}e^{-i\varphi_{\mathbf{p}}} - T_{AB}e^{i\varphi_{\mathbf{p}}}] / 2$, where $\varphi_{\mathbf{p}}$ is the direction of a momentum \mathbf{p} , and an isotropic part

$t_S(\mathbf{r}) = -iT_{AA}(\mathbf{r}) \sin(\theta/2)$ independent of $\varphi_{\mathbf{p}}$ that can be neglected [47] for $\theta \ll 1$. The resulting local spectrum $\epsilon_{\mathbf{p}\pm} = \pm \sqrt{(vp - u)^2 + \Delta_{\mathbf{p}}^2}$ has an anisotropic gap

$$\Delta_{\mathbf{p}}^2 = \delta_-^2 \cos^2[\varphi_{\mathbf{p}} - \Theta] + \delta_+^2 \sin^2[\varphi_{\mathbf{p}} - \Theta]. \quad (4)$$

which achieves minima $|\delta_-| = (|T_{AB}| - |T_{BA}|)/2$ at momentum orientations $\varphi_I = \Theta$ and $\varphi_{II} = \Theta + \pi$, where $\Theta(\mathbf{r}) = (\arg[T_{BA}] - \arg[T_{AB}])/2$. The gap is maximized at $\delta_+(\mathbf{r}) = (|T_{BA}| + |T_{AB}|)/2$ at the two perpendicular orientations.

It follows from the preceding analysis that the gap in the local electronic spectrum (4) closes if $|T_{AB}| = |T_{BA}|$. This condition is satisfied along the domain walls specified by dashed lines in Fig. 2-(a), where we illustrate the spatial pattern of $\delta_-(\mathbf{r})$. The domain walls separate regions where the inter-layer hybridization is dominated by the T_{AB} from regions in which it is dominated by T_{BA} . The local valley Chern number of Hamiltonian (3)

$$C = \int \frac{d\mathbf{p}}{4\pi} \mathbf{d} \left[\frac{\partial \mathbf{d}}{\partial p_x} \times \frac{\partial \mathbf{d}}{\partial p_y} \right] = \frac{\delta_-}{|\delta_-|}, \quad (5)$$

where $\mathbf{d} = \mathbf{h}/h$ and the vector \mathbf{h} is defined by the Pauli matrix expansion of Eq. (3), $H = (\boldsymbol{\sigma} \cdot \mathbf{h})$. The valley Chern number difference across the domain wall is $C_{AB} - C_{BA} = 2$, guaranteeing that two helical electronic channels are present in the gaps per valley and per spin.

In the vicinity of each domain wall the low-energy states are concentrated around the minima at orientations $\varphi_{I(II)}$, which are perpendicular to the domain wall, as illustrated in Fig. 2-(b). The expansion of the Hamiltonian (3) in the vicinity of these minima results in a pair of identical anisotropic Dirac cones with spatially depended mass $\delta_-(\mathbf{r})$:

$$H_D = \begin{pmatrix} \delta_-(\mathbf{r}) & vp_\perp - iv_{||}p_{||} \\ vp_\perp + iv_{||}p_{||} & -\delta_-(\mathbf{r}) \end{pmatrix}. \quad (6)$$

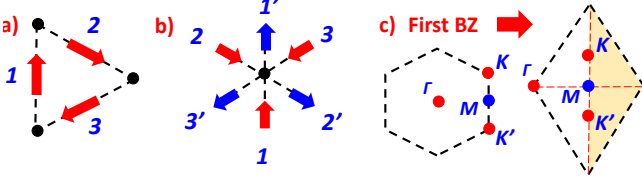


FIG. 3. (a) Elementary cell of the network. The wavefunction amplitudes are links 1, 2 and 3 are $\psi_{ij} = \{\psi_{ij}^1, \psi_{ij}^2, \psi_{ij}^3\}$. (b) Node with three incoming and three outgoing channels characterized by the scattering matrix T . (c) First Brillouin zone of the network in hexagonal and rhombohedral representations.

Here the velocity for momenta p_{\perp} perpendicular to the domain wall is the single-layer graphene Dirac velocity v . The velocity for momenta p_{\parallel} along the domain wall can be approximated by its value at the domain wall center $v_{\parallel} = \delta_{+}/p_{\perp} \approx 2wv/3u$. Each Dirac point carries one half of the valley Chern number $C_D = \delta_{-}/2|\delta_{-}|$, and is responsible for a single helical state. The Dirac mass $\delta_{-}(\mathbf{r})$ changes sign across the domain wall and Eq.(6) therefore has a Jackiw-Rebbi [48] solution that describes helical electronic states with dispersion $\epsilon_{p_{\parallel}} = v_{\parallel}p_{\parallel}$, and wave function

$$\psi_{p_{\parallel}}(r_{\perp}) = N \begin{pmatrix} 1 \\ i \end{pmatrix} \exp \left[i \frac{p_{\parallel} r_{\perp}}{\hbar} - \frac{wL}{\pi \hbar v} \sin^2 \left(\frac{\pi r_{\perp}}{\sqrt{3}L} \right) \right], \quad (7)$$

where N is a normalization factor. The center of AB/BA region, where wave functions of helical states from different domain walls overlap, are distanced at length $r_{\perp}^0 = L/2\sqrt{3}$ from them. The domain wall network is well developed if the overlap of wave functions $|\psi_{p_{\parallel}}(r_{\perp}^0)|^2/|\psi_{p_{\parallel}}(0)|^2 = \exp[-w/\epsilon_L] \ll 1$ is weak. Here $\epsilon_L = 2\pi\hbar v/L$ is the character energy scale of the moiré pattern.

These helical states are the only electronic degrees of freedom present when $|\epsilon| \ll u, w$. Three sets of parallel domain walls with orientations differing by 120° surround AB and BA regions and intersect at a set of points with local AA stacking. The considerations we have discussed to this point establish the physical picture we use to motivate our phenomenological helical network model for domain wall states.

Phenomenological network model— Our phenomenological helical network model consists of the links and nodes illustrated in Fig. 3-(a) and (b), which connect to form the domain wall pattern. We assume ballistic propagation along links and scattering only at nodes. The dis-

person law along links, $\epsilon = v_{\parallel}q$, is consistent with the Jackiw-Rebbi confined mode solution. For $\epsilon_L \ll w \lesssim u$, the two Dirac cones on opposite sides of the ring at φ_I and φ_{II} are well separated, allowing scattering between them to be neglected. This simplification allows us to consider a network with a single helical channel per link.

The full domain wall network can be constructed by placing the set of three elementary nodes on a triangular lattice with elementary lattice vectors $\mathbf{l}_{1,2} = L(\pm\sqrt{3}\mathbf{e}_x + \mathbf{e}_y)/2$. The wavefunction amplitudes on links 1, 2 and 3 of the cell centered at $\mathbf{R}_{ij} = i\mathbf{l}_1 + j\mathbf{l}_2$ are denoted by $\psi_{ij} = \{\psi_{ij}^1, \psi_{ij}^2, \psi_{ij}^3\}$. Each node has three input and three output channels and therefore has a 3×3 unitary scattering matrix T whose detailed form depends in a complex way [49] on the spatial profile of the domain walls intersection. We follow a simpler phenomenological approach. By observing that the straight-forward scattering amplitudes $|T_{11}| = |T_{22}| = |T_{33}|$ and the 240° deflection scattering amplitudes $|T_{12}| = |T_{13}| = |T_{21}| = |T_{23}| = |T_{31}| = |T_{32}|$ must be equal due to symmetry, it follows that the unitary matrix T can be parametrized by an angle α ranging between 0 and $\alpha_M = \arccos[1/3]$, and 6 phases $\phi_T, \phi_1^R, \phi_1^L, \phi_2^R, \phi_2^L, \phi_3$ ranging between 0 and 2π : $T = e^{i\phi_T} T_{\phi}^L \bar{T} T_{\phi}^R$, where ϕ_T is the average phase shift; $T_{\phi}^L = \text{diag}[e^{i(\phi_2^R + \phi_1^R + \phi_3)}, e^{-i\phi_2^L}, e^{-i\phi_1^L}]$ and $T_{\phi}^R = \text{diag}[e^{i(\phi_2^L + \phi_1^L - \phi_3)}, e^{-i\phi_2^R}, e^{-i\phi_1^R}]$ are phase shifts before and after scattering, which are not independent, and \bar{T} is the unitary matrix

$$\bar{T} = \begin{pmatrix} \cos \alpha e^{i\chi} & \frac{\sin \alpha}{\sqrt{2}} & \frac{\sin \alpha}{\sqrt{2}} \\ \frac{\sin \alpha}{\sqrt{2}} & -\frac{1 + \cos \alpha e^{-i\chi}}{2} & \frac{1 - \cos \alpha e^{-i\chi}}{2} \\ \frac{\sin \alpha}{\sqrt{2}} & \frac{1 - \cos \alpha e^{-i\chi}}{2} & -\frac{1 + \cos \alpha e^{-i\chi}}{2} \end{pmatrix}. \quad (8)$$

Here $\chi = \arccos[\{3\cos^2(\alpha) - 1\}/2\cos(\alpha)]$. The angle α defines the ratio of scattering probabilities between forward P_f and deflected P_d channels by $P_f/P_d = 2\cot^2(\alpha)$.

The outgoing and incoming electronic waves at a node are connected by $\psi_{\text{out}} = e^{-i\phi_E} T \psi_{\text{in}}$, where $\psi_{\text{out}} = (\psi_{i+1,j}^1, \psi_{i,j-1}^2, \psi_{i,j}^3)$ and $\psi_{\text{in}} = (\psi_{i,j-1}^1, \psi_{i,j}^2, \psi_{i+1,j}^3)$. Here $\phi_E = \epsilon L/\hbar v_{\parallel}$ is the dynamical phase accumulated by electrons while propagating between links. Bloch's theorem connects wave function amplitudes in different cells by $\psi_{ij} = e^{i\mathbf{q}\mathbf{R}_{ij}} \bar{\psi}$, where $\bar{\psi} \equiv \{\bar{\psi}^1, \bar{\psi}^2, \bar{\psi}^3\}$ and \mathbf{q} is the moiré momentum. The connection between input and output waves can be written as $[\lambda - U_{\mathbf{q}}] \bar{\psi} = 0$, and has a nontrivial solution only if $\lambda = e^{i(\phi_E - \phi_T)}$ is equal to one of eigenvalues of the matrix

$$U_{\mathbf{q}} = \begin{pmatrix} \cos \alpha e^{i(\chi + \phi_1^R + \phi_2^R + \phi_1^L + \phi_2^L - \mathbf{q}\mathbf{l}_1 - \mathbf{q}\mathbf{l}_2)} & \frac{\sin \alpha}{\sqrt{2}} e^{i(\phi_1^R + \phi_3 - \mathbf{q}\mathbf{l}_1)} & \frac{\sin \alpha}{\sqrt{2}} e^{i(\phi_2^R + \phi_3)} \\ \frac{\sin \alpha}{\sqrt{2}} e^{i(\phi_1^L - \phi_3)} & -\frac{1 + \cos \alpha e^{-i\chi}}{2} e^{i(\mathbf{q}\mathbf{l}_2 - \phi_2^R - \phi_1^L)} & \frac{1 - \cos \alpha e^{-i\chi}}{2} e^{i(\mathbf{q}\mathbf{l}_1 + \mathbf{q}\mathbf{l}_2 - \phi_1^R - \phi_2^L)} \\ \frac{\sin \alpha}{\sqrt{2}} e^{i(\phi_2^L - \phi_3 - \mathbf{q}\mathbf{l}_2)} & \frac{1 - \cos \alpha e^{-i\chi}}{2} e^{-i(\phi_2^R + \phi_1^L)} & -\frac{1 + \cos \alpha e^{-i\chi}}{2} e^{i(\mathbf{q}\mathbf{l}_1 - \phi_1^R - \phi_1^L)} \end{pmatrix}. \quad (9)$$

It follows that the electronic spectrum consists of groups of three bands $n = -1, 0, 1$ that repeat in energy with period $\epsilon_L^{\parallel} = 2\pi\hbar v_{\parallel}/L$ and have dispersion

$$\epsilon_{\mathbf{q}}^{nm} = \epsilon_L^{\parallel} \left(\frac{\arg[\lambda_{\mathbf{q}}^n]}{2\pi} + \frac{\phi_T}{2\pi} + m \right). \quad (10)$$

Here $\lambda_{\mathbf{q}}^n$ are the eigenvalues of $U_{\mathbf{q}}$ and m is an integer. The role of the phase ϕ_T is just a rigid shifts of all bands in energy. Since the matrix $U_{\mathbf{q}}$ is also unitary $U_{\mathbf{q}}^{\dagger} = U_{\mathbf{q}}^{-1}$ and $\det[U_{\mathbf{q}}] = 1$, its eigenvalues satisfy

$$\lambda_{\mathbf{q}}^3 - \text{tr}[U_{\mathbf{q}}]\lambda_{\mathbf{q}}^2 + \text{tr}[U_{\mathbf{q}}^{\dagger}]\lambda_{\mathbf{q}} - 1 = 0. \quad (11)$$

The electronic spectrum therefore depends only on

$$\begin{aligned} \text{tr}[U_{\mathbf{q}}] &= \cos(\alpha) e^{i\chi} e^{i(\Phi_1 + \Phi_2 - \mathbf{q}\mathbf{l}_1 - \mathbf{q}\mathbf{l}_2)} \\ &- \frac{1}{2} [1 + \cos(\alpha) e^{-i\chi}] \left[e^{i(\mathbf{q}\mathbf{l}_1 - \Phi_1)} + e^{i(\mathbf{q}\mathbf{l}_2 - \Phi_2)} \right]. \end{aligned} \quad (12)$$

Here we have introduced phases $\Phi_1 = \phi_1^L + \phi_1^R$, $\Phi_2 = \phi_2^L + \phi_2^R$. These phases Φ_1 and Φ_2 can be eliminated by the shift of the momentum space origin, and therefore do not influence the density of states of the network and electronic transport through it. The latter remarkably depend only on α , which in turn characterizes the distribution of scattering probability between forward and deflected channels. It has been numerically shown [50] that, contrary to classical intuition, because nearby paths have larger wavefunction overlap with the incoming electron, deflection is the more likely outcome. For presentation of results we chose $\alpha = 1.1$ corresponding to $P_f \approx 0.2$ and $P_d \approx 0.4$.

The first Brillouin zone of the network has a hexagonal shape and is illustrated in Fig.3-c where we also

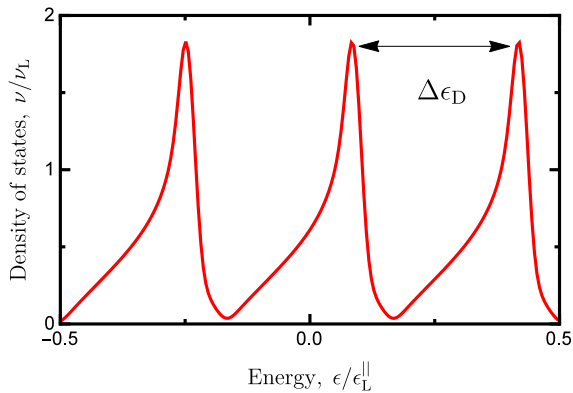


FIG. 4. The energy dependence of the density of states $\nu(\epsilon)$ per valley, spin and per Dirac point in the ring. It has three dips and three maxima separated from each other by $\Delta\epsilon_D = \epsilon_L^{\parallel}/3$. The primer correspond to Dirac points, while the latter to saddle points of the moiré pattern band structure presented in Fig. 1. The corresponding scale for the density of states is $\nu_L = \sqrt{3}\pi/\epsilon_L^{\parallel} L^2$.

illustrate an equivalent rhombic primitive cell. The spectrum has the mirror symmetry across the KK' line since $\text{tr}[U_{q_M - q_x, q_y}] = \text{tr}[U_{q_M + q_x, q_y}]$, where $\mathbf{q}_M = 2\pi\mathbf{e}_x/\sqrt{3}L$ is the position of the M-point in the Brillouin zone. For presentation of results we have chosen $\phi_T = \Phi_1 = \Phi_2 = (\pi - 2 \arcsin[3 \sin \alpha / 2\sqrt{2}])/3$ that ensures the discrete rotational symmetry of the network band structure with respect to 120° around the Γ -point. A single period $\epsilon_{\mathbf{q}}^{n0}$ of the repeating band structure is plotted in the half of the rhombic Brillouin zone in Fig. 1, where we see that it is gapless because of Dirac band touching points situated in Γ , K, and K' high symmetry points. Their positions are independent on α and they are separated by momentum $\Delta k_D = 4\pi/3L$ and energy $\Delta\epsilon_D = \epsilon_L^{\parallel}/3$. The density of states of the network is presented in Fig. 4 and is periodic with period $\Delta\epsilon_D$. It is three time smaller than the period of the network band structure ϵ_L^{\parallel} , that reflects the symmetry between three links in an elementary cell of the model. The single period contains one zero at the Dirac point, and one saddle-point logarithmic divergence. The latter reflects the van Hove singularity due to the presence of saddle points in the network band structure, which are clearly visible in Fig. 1.

In recent experiments [20] the small twist-angle $\theta = 0.245^\circ$ has been applied between layers and has resulted in moiré patterns with period $L \approx 58$ nm. The resulting energy scale of the pattern $\epsilon_L = 2\pi\hbar v/L \approx 72$ meV is comparable with the induced gap $\epsilon_g \approx 60$ meV. While the phenomenological network model is still reasonable at energies $\epsilon \ll \epsilon_g$, the expressions for v_{\parallel} and $\Delta\epsilon_D$ do not directly apply. Our model predicts the periodic set of features in the density of states, whereas only one feature within the gap has been observed [20]. For the gap $\epsilon_g \approx 250$ meV achievable in bilayer graphene [51, 52], our model is well applicable in much wider range of energies. Using the hybridization energy $w = 400$ meV we get that the velocity of helical states $v_{\parallel} = 1.6 \cdot 10^6$ m/s is larger than the velocity of electrons in graphene $v = 10^6$ m/s. The period of the network is equal to $\epsilon_L^{\parallel} \approx 115$ meV and the the period of density of states $\Delta\epsilon_D \approx 38$ meV. It is much smaller than the gap ϵ_g and we expect a set of features due to van Hove singularities of network spectrum to be well resolved in experiments. Alternatively, the condition $\epsilon_L^{\parallel} \ll \epsilon_g$ can be achieved at smaller twist angles θ .

To conclude, we have introduced a new phenomenological network model which captures the electronic structure of twisted bilayer graphene in the energy range below the AB and BA gaps where only topologically confined domain wall states are present. Motivated by the recent observation of the domain wall network in STM experiments [20] we have focused on its band structure and density of states. Very recently signatures of the network formation have been found in magneto-transport experiments [53]. Whereas our model predicts anisotropic

transport properties that are approximately periodic in carrier density, the magneto-transport theory is postponed for future work.

Acknowledgment. This material is based upon work supported by the Department of Energy under Grant No DE-FG02-ER45118 and by the Welch Foundation under Grant No. F1473.

-
- [1] E. McCann and M. Koshino, *Rep. Prog. Phys.* **76**, 056503 (2013).
- [2] A. Rozhkov, A. Sboychakov, A. Rakhmanov, and F. Nori, *Phys. Rep.* **648**, 1 (2016).
- [3] I. Martin, Y. M. Blanter, and A. F. Morpurgo, *Phys. Rev. Lett.* **100**, 036804 (2008).
- [4] A. S. Nunez, E. S. Morell, and P. Vargas, *Appl. Phys. Lett.* **98**, 262107 (2011).
- [5] D. A. Cosma and V. I. Fal'ko, *Phys. Rev. B* **92**, 165412 (2015).
- [6] D. R. da Costa, A. Chaves, S. H. R. Sena, G. A. Farias, and F. M. Peeters, *Phys. Rev. B* **92**, 045417 (2015).
- [7] F. Zhang, A. H. MacDonald, and E. J. Mele, *Proc. Natl. Acad. Sci. USA* **110**, 10546 (2013).
- [8] A. Vaezi, Y. Liang, D. H. Ngai, L. Yang, and E.-A. Kim, *Phys. Rev. X* **3**, 021018 (2013).
- [9] M. Koshino, *Phys. Rev. B* **88**, 115409 (2013).
- [10] L.-J. Yin, H. Jiang, J.-B. Qiao, and L. He, *Nat. Commun.* **7**, 11760 (2016).
- [11] L. Ju, Z. Shi, N. Nair, Y. Lv, C. Jin, J. Velasco Jr, C. Ojeda-Aristizabal, H. A. Bechtel, M. C. Martin, A. Zettl, J. Analytis, and F. Wang, *Nature* **520**, 650 (2015).
- [12] J. Li, K. Wang, K. J. McFaul, Z. Zern, Y. Ren, K. Watanabe, T. Taniguchi, Z. Qiao, and J. Zhu, *Nat. Nano* **11**, 1060 (2016).
- [13] Z. Qiao, J. Jung, Q. Niu, and A. H. MacDonald, *Nano Lett.* **11**, 3453 (2011).
- [14] Z. Qiao, J. Jung, C. Lin, Y. Ren, A. H. MacDonald, and Q. Niu, *Phys. Rev. Lett.* **112**, 206601 (2014).
- [15] H. Pan, X. Li, F. Zhang, and S. A. Yang, *Phys. Rev. B* **92**, 041404 (2015).
- [16] A. R. Wright and T. Hyart, *Appl. Phys. Lett.* **98**, 251902 (2011).
- [17] Y. Ren, J. Zeng, K. Wang, F. Xu, and Z. Qiao, ArXiv e-prints [arXiv:1708.02700](https://arxiv.org/abs/1708.02700) (2017).
- [18] V. Mosallanejad, K. Wang, Z. Qiao, and G. Guo, ArXiv e-prints [arXiv:1704.01504](https://arxiv.org/abs/1704.01504) (2017).
- [19] Y. Ren, Z. Qiao, and Q. Niu, *Rep. Prog. Phys.* **79**, 066501 (2016).
- [20] S. Huang, K. Kim, D. K. Efimkin, T. Lovorn, T. Taniguchi, K. Watanabe, A. H. MacDonald, E. Tutuc, and B. J. LeRoy, ArXiv e-prints (2018), [arXiv:1802.02999](https://arxiv.org/abs/1802.02999) [cond-mat.mes-hall].
- [21] R. Bistritzer and A. H. MacDonald, *Proc. Natl. Acad. Sci. US* **108**, 12233 (2011).
- [22] J. Jung, A. Raoux, Z. Qiao, and A. H. MacDonald, *Phys. Rev. B* **89**, 205414 (2014).
- [23] A. V. Rozhkov, A. O. Sboychakov, A. L. Rakhmanov, and F. Nori, *Phys. Rev. B* **95**, 045119 (2017).
- [24] D. Weckbecker, S. Shallcross, M. Fleischmann, N. Ray, S. Sharma, and O. Pankratov, *Phys. Rev. B* **93**, 035452 (2016).
- [25] J. M. B. Lopes dos Santos, N. M. R. Peres, and A. H. Castro Neto, *Phys. Rev. B* **86**, 155449 (2012).
- [26] J. M. B. Lopes dos Santos, N. M. R. Peres, and A. H. Castro Neto, *Phys. Rev. Lett.* **99**, 256802 (2007).
- [27] J. C. W. Song, P. Samutpraphoot, and L. S. Levitov, *Proc. Natl. Acad. Sci. US* **112**, 10879 (2015).
- [28] M. Mucha-Kruczyński, J. R. Wallbank, and V. I. Fal'ko, *Phys. Rev. B* **93**, 085409 (2016).
- [29] R. de Gail, M. O. Goerbig, F. Guinea, G. Montambaux, and A. H. Castro Neto, *Phys. Rev. B* **84**, 045436 (2011).
- [30] G. Trambly de Laissardière, D. Mayou, and L. Magaud, *Phys. Rev. B* **86**, 125413 (2012).
- [31] X. Bi, J. Jung, and Z. Qiao, *Phys. Rev. B* **92**, 235421 (2015).
- [32] G. Chen, M. Sui, D. Wang, S. Wang, J. Jung, P. Moon, S. Adam, K. Watanabe, T. Taniguchi, S. Zhou, M. Koshino, G. Zhang, and Y. Zhang, *Nano Lett.* **17**, 3576 (2017).
- [33] S. Dai, Y. Xiang, and D. J. Srolovitz, *Nano Lett.* **16**, 5923 (2016).
- [34] P. San-Jose, R. V. Gorbachev, A. K. Geim, K. S. Novoselov, and F. Guinea, *Nano Lett.* **14**, 2052 (2014).
- [35] V. Cherkaz, G. T. de Laissardière, P. Mallet, and J.-Y. Veuillen, *Phys. Rev. B* **91**, 155428 (2015).
- [36] Q. Yao, R. van Bremen, G. J. Slotman, L. Zhang, S. Haartsen, K. Sotthewes, P. Bampoulis, P. L. de Boeij, A. van Houselt, S. Yuan, and H. J. W. Zandvliet, *Phys. Rev. B* **95**, 245116 (2017).
- [37] J. S. Alden, A. W. Tsen, P. Y. Huang, R. Hovden, L. Brown, J. Park, D. A. Muller, and P. L. McEuen, *Proc. Natl. Acad. Sci. USA* **110**, 11256 (2013).
- [38] K. Kim, A. DaSilva, S. Huang, B. Fallahazad, S. Larentis, T. Taniguchi, K. Watanabe, B. J. LeRoy, A. H. MacDonald, and E. Tutuc, *Proc. Natl. Acad. Sci. USA* **114**, 3364 (2017).
- [39] F. Hu, S. R. Das, Y. Luan, T.-F. Chung, Y. P. Chen, and Z. Fei, *Phys. Rev. Lett.* **119**, 247402 (2017).
- [40] Y. Cao, V. Fatemi, S. Fang, K. Watanabe, T. Taniguchi, E. Kaxiras, and P. Jarillo-Herrero, *Nature* **10.1038/nature26160**.
- [41] P. San-Jose and E. Prada, *Phys. Rev. B* **88**, 121408 (2013).
- [42] G. Trambly de Laissardière, O. F. Namarvar, D. Mayou, and L. Magaud, *Phys. Rev. B* **93**, 235135 (2016).
- [43] J. T. Chalker and P. D. Coddington, *Journal of Physics C: Solid State Physics* **21**, 2665 (1988).
- [44] C.-M. Ho and J. T. Chalker, *Phys. Rev. B* **54**, 8708 (1996).
- [45] V. V. Mkhitaryan and M. E. Raikh, *Phys. Rev. B* **79**, 125401 (2009).
- [46] (), a geometry of the graphene bilayer needs to be characterized not only by a twist θ , but also by a relative translation vector \mathbf{d} . As it has been shown previously [21] the latter only shifts the moiré pattern, while its electronic band structure is independent on \mathbf{d} .
- [47] (), the isotropic contribution t_S is important only in the vicinity of domain wall intersections. In our phenomenological network model the scattering matrix for nodes T is parametrized in a phenomenological way and details of the intersections profile are off importance.
- [48] R. Jackiw and C. Rebbi, *Phys. Rev. D* **13**, 3398 (1976).
- [49] J. R. Anglin and A. Schulz, *Phys. Rev. B* **95**, 045430

- (2017).
- [50] Z. Qiao, J. Jung, C. Lin, Y. Ren, A. H. MacDonald, and Q. Niu, *Phys. Rev. Lett.* **112**, 206601 (2014).
 - [51] K. Kanayama and K. Nagashio, *Scientific Reports* **5**, 15789 (2015).
 - [52] Y. Zhang, T.-T. Tang, C. Girit, Z. Hao, M. C. Martin, A. Zettl, M. F. Crommie, Y. R. Shen, and F. Wang, *Nature* **459**, 820 (2017).
 - [53] P. Rickhaus, J. Wallbank, S. Slizovskiy, R. Pisoni, H. Overweg, Y. Lee, M. Eich, M.-H. Liu, K. Watanabe, T. Taniguchi, V. Fal'ko, T. Ihn, and K. Ensslin, ArXiv e-prints (2018), [arXiv:1802.07317 \[cond-mat.mes-hall\]](#).